Nano Research
2021, 14(12): 4789–4794
ISSN 1998-0124 CN 11-5974/O4
https://doi.org/10.1007/s12274-021-3429-5

Research Article

Novel vertically aligned nanocomposite of Bi_2WO_6-Co_3O_4 with room-temperature multiferroic and anisotropic optical response

Leigang Li[1,§], Shikhar Misra[1,§], Xingyao Gao[1], Juncheng Liu[1], Han Wang[1], Jijie Huang[1], Bruce Zhang[2], Ping Lu[3], and Haiyan Wang[1,2] (✉)

[1] School of Materials Engineering, Purdue University, West Lafayette, Indiana 47907, USA
[2] School of Electrical and Computer Engineering, Purdue University, West Lafayette, Indiana 47907, USA
[3] Sandia National Laboratory, Albuquerque, New Mexico 87185, USA
[§] Leigang Li and Shikhar Misra contributed equally to this work.

Received: 16 January 2021 / **Revised:** 24 February 2021 / **Accepted:** 26 February 2021

ABSTRACT

A new vertically aligned nanocomposite (VAN) structure based on two-dimensional (2D) layered oxides has been designed and self-assembled on both $LaAlO_3$ (001) and $SrTiO_3$ (001) substrates. The new VAN structure consists of epitaxially grown Co_3O_4 nanopillars embedded in the Bi_2WO_6 matrix with a unique 2D layered structure, as evidenced by the microstructural analysis. Physical property measurements show that the new Bi_2WO_6-Co_3O_4 VAN structure exhibits strong ferromagnetic and piezoelectric response at room temperature as well as anisotropic permittivity response. This work demonstrates a new approach in processing multifunctional VANs structure based on the layered oxide systems towards future nonlinear optics, ferromagnets, and multiferroics.

KEYWORDS

vertically aligned nanocomposite (VAN), multiferroics, Aurivillius oxides, layered oxides, Co_3O_4, Bi_2WO_6

1 Introduction

Multiferroics, with at least two ferroic orders coexisting in one phase, have stimulated a tremendous flurry of research interests because of the rich underlying physics and promising microelectronic applications [1–3]. A variety of multiferroic materials have been discovered and synthesized, including the single-phase multiferroics (e.g., $YMnO_3$ [4–7] and $BiFeO_3$ [3, 8–10]), vertical heterostructures (e.g., $BaTiO_3$-$CoFe_2O_4$ [11], $PbTiO_3$-$CoFe_2O_4$ [12, 13], $Bi_5Ti_3FeO_{15}$-$CoFe_2O_4$ [14]), and horizontal multilayer heterostructures (e.g., $La_{0.7}Ca_{0.3}MnO_3$/$BaTiO_3$ [15]). Single-phase multiferroic materials are still scarce despite of the very few single phase ones such as $YMnO_3$ [4–7] and $BiFeO_3$ [3, 8–10]. The scarcity of simultaneous ferroelectric and ferromagnetic ordering in a single phase is attributed to the contradicting mechanisms of ferroelectricity (requiring formally empty d orbitals) and magnetic moments (usually requiring partially filled d orbitals) [1]. Taking a single-phase bismuth ferrite ($BiFeO_3$) as an example, it exhibits extremely high ferroelectric polarization (90 μC/cm^2) [16], but its antiferromagnetic nature and weak ferromagnetism have hindered its practical applications [17].

Recently, the mechanism of creating ferroelectricity from the stereochemical activity of the 6s^2 lone pair on the large Bi^{3+} (A-site) and magnetism from the small Fe^{3+} cation (B-site) provides important clues of creating new multiferroic materials. A bismuth-based single-phase multiferroic $Bi_3Fe_2Mn_2O_{10-\delta}$ (BFMO322) in a novel layered supercell structure was reported [18–21]. The ferroelectricity and magnetism is believed to originate from the Bi^{3+} 6s^2 lone pairs and distorted FeO_6/MnO_6 octahedra, respectively. The highly anisotropic layered BFMO322 supercell structure renders highly anisotropic magnetic properties besides the ferroelectric polarization. Bi_2WO_6 (BWO), another bismuth-based layered oxide, is believed to be the simplest Aurivillius phase and possesses desirable room-temperature ferroelectricity [22–24]. The nonmagnetic W^{6+} cations, however, make it impossible to achieve multiferroism in this single-phase layered structure. Despite of this issue, the layered framework of BWO, in conjunction with the 6s^2 lone pairs of Bi^{3+}, is still appealing for the design of anisotropic multiferroic materials. In addition, Choi et al. have reported that the Aurivillius layered structure of $Bi_4Ti_3O_{12}$ can be preserved after being alloyed with $LaTMO_3$ (TM represents transition metals, TM = Co, Ni, Mn, Ti, etc.) [25, 26]. Their study indicates that Co is incorporated into the $Bi_4Ti_3O_{12}$ matrix by preferentially substituting Ti near to the Bi_2O_2 layer while maintaining the layered structure.

In this work, we propose to couple the layered BWO with bismuth-based transition metal oxides ($BiMO_3$, M = Co) to form a new multiferroic layered oxide system. It is expected that the magnetic element is "inserted" into the BWO matrix and the BWO layered structure can still be maintained. By the incorporation of magnetic element into the matrix, a layered multiferroic material should be created with the ferroelectricity originating from the Bi^{3+} 6s^2 lone pairs and the magnetism coming from the inserted magnetic elements. $BiCoO_3$ (BCO) was chosen as an example in this work to demonstrate the incorporation of Co into the BWO matrix for ferromagnetism.

Address correspondence to hwang00@purdue.edu

Instead of uniformly substituting W^{6+} by Co cations, however, the Co cations have segregated and a new material structure is formed showing the feature of vertically aligned nanocomposites (VANs) [27–33]. Different from the prior reported multilayered structures, VANs represent a new class of two-phase nanocomposite structures grown by a one-step self-assembly method, instead of the sequential deposition of two different materials in multilayers. To achieve VANs, careful materials selections are needed, such as good lattice matching of the two phases with the underlying substrate, good chemical and thermal stability, different surface energies, etc. Despite of these material selection requirements, the selection of VAN phases is more versatile than that of multilayer thin films. The VAN phases could include oxides, nitrides, metals, and others [34–36]. During PLD process, the different adatoms segregate and nucleate into two phases to minimize the overall surface energy of the material system. Furthermore, most of the prior reported VANs focus on perovskite oxides as the matrix material. In this work, we highlight a new class of VAN system using BWO layered oxide as the matrix. Coupled with the incorporation of the magnetic Co cations, strong ferromagnetism along with robust ferroelectric properties are expected at room temperature. The study could pave a new avenue towards the design of new room-temperature multiferroic materials.

2 Experimental

The targets used for thin film growth were prepared by a solid-state sintering method. More specifically, the powders of Bi_2O_3 and WO_3 (molar ratio, Bi:W = 2:1) were mixed, pressed into a pellet, and sintered at 700 °C for 3 hours in air. For Bi_2WO_6-Co_3O_4 composite target, the powders of Bi_2O_3, WO_3, and Co_3O_4 (molar ratio, Bi:W:Co = 3:1:1) were mixed, pressed and sintered at 700 °C for 3 hours in air. The epitaxial thin films were grown on both $LaAlO_3$ (LAO) (001) and $SrTiO_3$ (STO) (001) substrates using a pulsed laser deposition (PLD) method with a KrF excimer laser (Lambda Physik Compex Pro 205, λ = 248 nm). An optimized substrate temperature of 600 °C was used for the deposition of Bi_2WO_6 and Bi_2WO_6-Co_3O_4 thin films, respectively. The oxygen pressure in the chamber is 200 mTorr, the energy density is 400 mJ, the laser frequency is 2 Hz, and the deposition time is 20 min. After deposition, the films were annealed in the chamber at 400 °C for 1 hour under an oxygen pressure of 500 Torr and then cooled down to room temperature. $La_{0.7}Sr_{0.3}MnO_3$ (LSMO) buffer layer was deposited at 750 °C and 200 mTorr as the bottom electrode.

The microstructure of the thin films was investigated by X-ray diffraction (XRD, PANalytical Empyrean) and transmission electron microscopy (TEM, FEI Tecnai G2 F20 ST Materials). The scanning transmission electron microscopy (STEM) images in high-angle annular dark-field (HAADF) mode were recorded by a FEI Titan™ G2 80-200 microscope with a Cs probe corrector. A FEI Titan™ G2 80-200 STEM with a Cs probe corrector and ChemiSTEM™ technology operated at 200 kV was used in this study for energy-dispersive X-ray spectroscopy (EDS) chemical mapping [37, 38]. The samples used for TEM and STEM analysis were prepared by a standard manual grinding and thinning procedure followed by final ion polishing in a precision ion polishing system (PIPS 691, Gatan).

The magnetic properties of the thin films were investigated using the vibrating sample magnetometer (VSM) option in a commercial Physical Properties Measurement System (PPMS 6000, Quantum Design). During the measurement, the out-of-plane and in-plane magnetization were recorded by applying a magnetic field of 1 T perpendicular and parallel to the film plane, respectively. During the zero-field cooling (ZFC) measurement, the samples were cooled down from 380 to 10 K without a magnetic field and the magnetizations were then recorded during heating the samples to 380 K. In the case of field cooling (FC) measurement, the samples were cooled down from 380 to 10 K in a magnetic field (1,000 Oe) and the magnetizations were recorded when increasing the temperature to 380 K. The piezoelectric properties were measured at ambient conditions with a conductive Pt-Ir coated Si tip (model: SCM-PIT) via the Bruker Dimension atomic force microscope (AFM). The optical property was measured by UV–Vis–NIR Lambda 1050 spectrometer. The permittivity measurements were performed using angular dependent spectroscopic ellipsometer (JA Woollam RC2) and the model was fit to the ellipsometer data using CompleteEASE.

3 Results and discussion

The BWO-Co_3O_4 composite thin films were grown on various substrates by a one-step pulsed laser deposition method. VAN thin film was obtained as illustrated in Figs. 1(a) and 1(b). The epitaxial thin film growth was first investigated by high-resolution X-ray diffraction (XRD). The highly textured growth of BWO and BWO-Co_3O_4 VAN thin films on $LaAlO_3$ (LAO) (001) is shown by the dominant (00l)-type diffraction peaks in the XRD θ–2θ scans (Figs. 1(c) and 1(d)). The similar peak positions of BWO and BWO-Co_3O_4 VAN thin film may indicate that the layered structure of BWO on LAO is preserved after being alloyed with BCO. Furthermore, the insertion of Co_3O_4 phase into BWO has suppressed the growth of impurity phases (e.g., Bi_2O_3) as indicated from the comparison of BWO and BWO-Co_3O_4 θ–2θ scans. The dominant diffraction peaks shown in Figs. S1(a) and S1(b) in the ESM indicate that the BWO-Co_3O_4 VAN thin film can also be well grown on $SrTiO_3$ (STO) (001) and LSMO-buffered STO substrates.

The microstructure of BWO and BWO-Co_3O_4 VAN thin films was further characterized by TEM/STEM coupled with EDS analysis as shown in Figs. 2 and 3. Figure 2(a) displays the STEM image of the BWO thin film grown on LAO (001) obtained in HAADF mode. The sharp diffraction dots in the selected area electron diffraction pattern (SAED) in the inset of Fig. 2(a)) signifies the highly epitaxial growth of BWO film on LAO (001). The BWO thin film grows on LAO (001) substrate in a highly epitaxial manner with two sublattices of W-O octahedral layers and Bi_2O_2 sheets stacking alternatively along the film's growth direction (Fig. 2(b)). Figures 2(c) and 2(d)

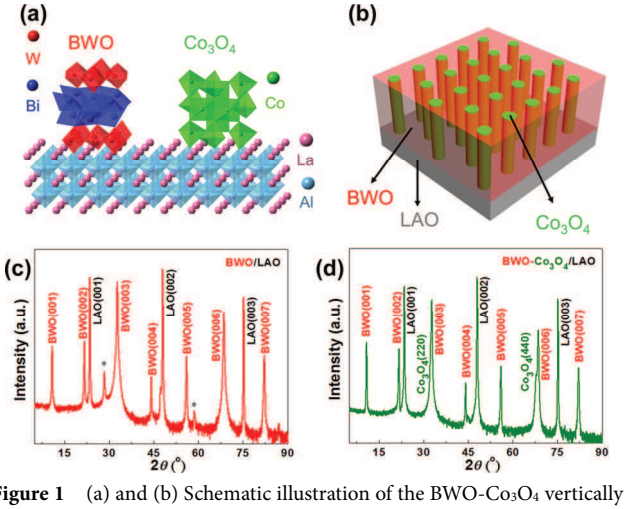

Figure 1 (a) and (b) Schematic illustration of the BWO-Co_3O_4 vertically aligned nanocomposite. XRD θ–2θ patterns of (c) BWO and (d) BWO-Co_3O_4 grown on LAO (001) substrate. The symbol "*" indicates the impure phase Bi_2O_3.

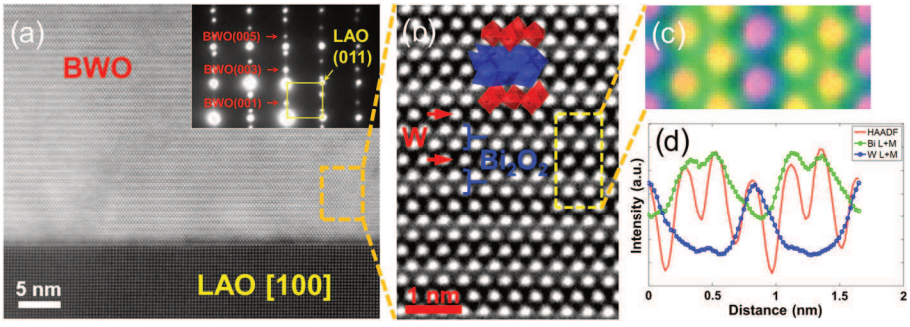

Figure 2 (a) STEM HAADF image of BWO thin film taken along LAO [100] zone axis. The inset shows the SAED pattern. (b) High-resolution STEM HAADF image showing the one-layer-thick W–O and two-layer-thick Bi–O. The inset is a schematic drawing of BWO. High-resolution EDS (c) mapping and (d) line scan confirming the chemical composition of BWO.

demonstrate the high-resolution EDS mapping and intensity profile of BWO, respectively, which confirms the microstructure and chemical composition of the BWO thin film.

Figure 3(b) shows the cross-sectional STEM HAADF image of BWO-Co_3O_4 thin film grown on LAO (001) substrate. The STEM image clearly demonstrates a two-phase growth mode of the BWO-Co_3O_4 thin film on LAO (001) substrate (Fig. 3(a)) evidenced by the different contrast from the vertical pillars and the matrix. More specifically, a 2-phase nanocomposite thin film with aligned vertically nanopillars, has been created, showing similar microstructure characteristics to the widely studied vertically aligned nanocomposite (VAN) thin films [28–30, 34, 39–41]. Much more vertical interfaces can be created for VANs than traditional multilayer thin films which can be employed for strain coupling along the vertical direction and functionality tuning. The strain tuning in VANs can be extended to several tens and even several hundreds of nanometers which brings more opportunities in achieving novel functionalities. Typical thin film strain induced from the underlayer is limited to the critical thickness which is about few nanometers. Furthermore, the primary difference of this work is the layered oxide BWO as the matrix, instead of the well reported cubic or pseudo-cubic structured oxides as the matrix in other VANs. The dominant diffraction patterns in the inset of Fig. 3(b) displays the highly epitaxial growth of BWO-Co_3O_4 VAN thin film along the film growth direction on LAO (001) substrate. The high-resolution STEM image in Fig. 3(c) shows a typical Co_3O_4 nanopillar in BWO matrix. The dark contrast phase is attributed to Co-rich phase (Co_3O_4) while the bright contrast one is W-rich phase (BWO) because of the heavier element of W (Z_W = 74) than that of Co (Z_{Co} = 27). To better demonstrate the microstructure of the film, high-resolution EDS mapping was performed on the sample. Figure 3(e) demonstrates the EDS mapping image of the region in Fig. 3(d) which displays Co-rich columns (in green) embedded in the BWO matrix (in red). Plan-view TEM image and EDS mapping were obtained to further characterize the Co-rich nanopillars surrounded by BWO matrix as shown in Figs. 3(f) to 3(j). Based on the EDS mapping for Bi in Fig. 3(i), we can clearly see that there is no distribution of Bi at the part for Co-containing areas. Therefore, it can be confirmed that the second phase did not contain Bi and thus it is identified as the Co_3O_4 area. The plan-view STEM image (Fig. 3(f)) coupled with the corresponding EDS mapping (Figs. 3(g) to 3(j)) further confirms the microstructure

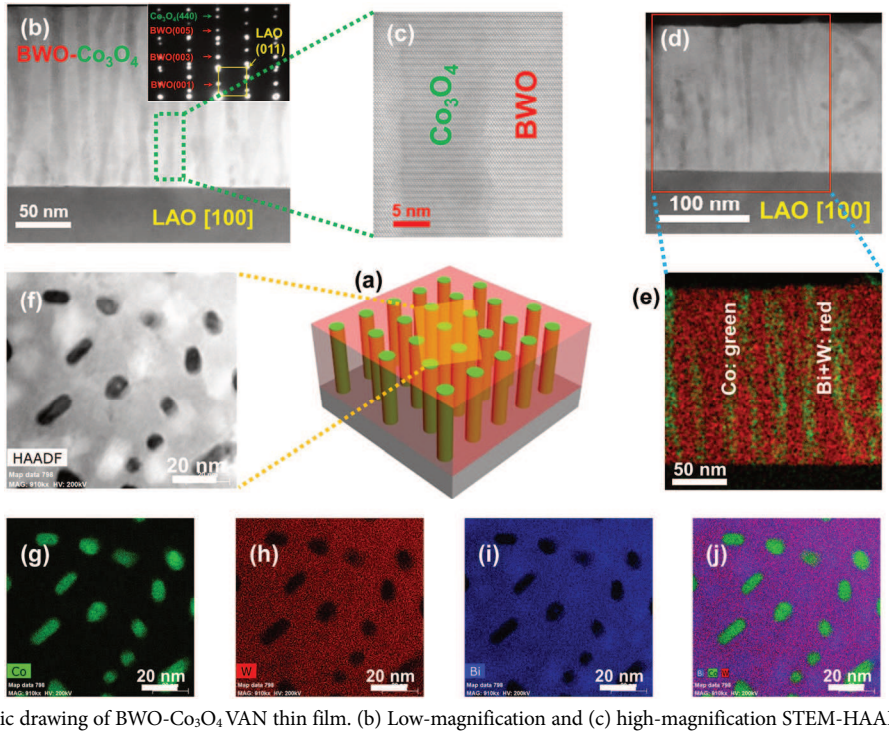

Figure 3 (a) A schematic drawing of BWO-Co_3O_4 VAN thin film. (b) Low-magnification and (c) high-magnification STEM-HAADF image of BWO-Co_3O_4 VAN thin film taken along LAO [100] zone axis. The inset in (b) shows the SAED pattern. (d) STEM HAADF image and (e) cross-section EDS mapping of BWO-Co_3O_4 VAN thin film acquired from the marked area in (d). (f) Plan-view STEM image and ((g), (h), (i), (j)) EDS mapping of BWO-Co_3O_4 VAN thin film showing the Co_3O_4 nanopillars embedded in the BWO matrix.

of BWO-Co_3O_4 VAN thin film. The surface morphology of the thin film was acquired by atomic force microscopy (AFM) image and an average surface roughness of 1.8 nm was obtained (Fig. S2 in the ESM).

With the fascinating VAN structure formed by the integration of the magnetic Co element into the Bi-W-O matrix, magnetism is expected for the BWO-Co_3O_4 VAN thin film. The magnetic properties of the BWO-Co_3O_4 VAN (~ 186 nm) thin film were measured by the PPMS with a VSM. Figure 4(a) presents the in-plane (IP) and out-of-plane (OP) magnetization hysteresis loops of BWO-Co_3O_4 VAN thin film by applying a magnetic field parallel and perpendicular to the film plane, respectively. The IP and OP saturation magnetization at 300 K and 3 kOe are ~ 94 and ~ 67 emu/cc, respectively, signifying strong ferromagnetism at room temperature. The coercivity for the BWO-Co_3O_4 VAN thin film along IP and OP direction both is ~ 229 Oe. The ferromagnetic property of BWO-Co_3O_4 VAN thin film is superior or comparable to that of prior reported magnetic materials as listed in Table S1 in the ESM. Different from the BWO-Co_3O_4 VAN thin film with strong room-temperature ferromagnetism, the BWO thin film (~ 192 nm) shows no ferromagnetic response at room temperature as shown in Fig. 4(c). Furthermore, the BWO-Co_3O_4 VAN thin film shows strong ferromagnetic response above room temperature as indicated by the temperature-dependent magnetization measurement in Fig. 4(b). A common characteristic for Bi-containing compounds, including the Aurivillius phases, is that a localized lobe-like distribution of $6s^2$ lone-pair electrons exist which breaks the spatial inversion symmetry and become the driving force for ferroelectric structural distortion [42–44]. The ferroelectric property of BWO-Co_3O_4 VAN thin film in this work is referenced to the piezoelectric response. Figure 4(d) shows the out-of-plane amplitude and phase switching curves with a DC voltage applied through the tip to bias the sample (0.25 cm^2). The sharp 180° phase change and amplitude switching curve as well as the polarization loop indicate obvious ferroelectric domain switching in the BWO-Co_3O_4 VAN thin film grown on LSMO (~ 10 nm) buffered STO substrate (Fig. S3 in the ESM). Both the strong ferromagnetism and piezoelectric response of the BWO-Co_3O_4 VAN structure, formed by the introduction of magnetic Co element into the Bi_2WO_6 matrix, make it a promising room-temperature multiferroic material.

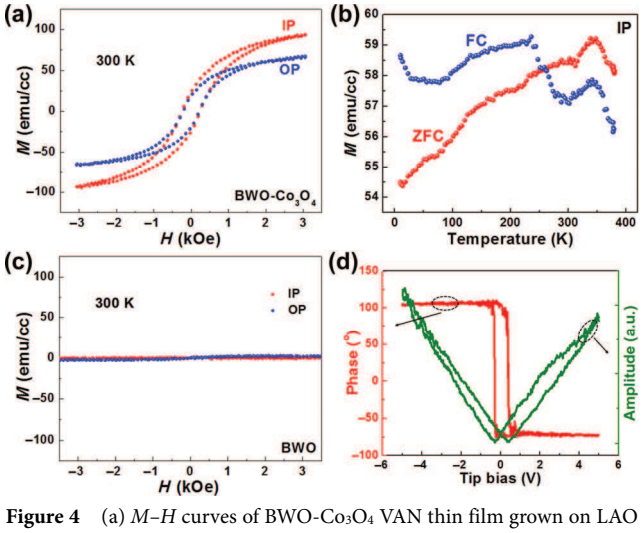

Figure 4 (a) *M*–*H* curves of BWO-Co_3O_4 VAN thin film grown on LAO substrate. (b) *M*–*T* curves of BWO-Co_3O_4 VAN thin film acquired under FC and ZFC conditions. (c) *M*–*H* curves of BWO thin film grown on LAO substrate. (d) Phase and amplitude switching curves of BWO-Co_3O_4 VAN thin film grown on LSMO buffered STO substrate.

Regarding the anisotropic layered phase and the VAN structure, it is highly attractive to explore the optical response of the BWO-Co_3O_4 VAN structure and BWO sample. UV–Vis–NIR Lambda 1050 spectrometer was employed to measure the optical properties both under direct incident light and tilted light with different angles. Figure 5(a) presents the optical transmission spectra of both BWO-Co_3O_4 VAN (~ 186 nm) and BWO (~ 192 nm) thin films as a function of wavelength under normal incident light. The spectrum of both BWO-Co_3O_4 VAN and BWO thin films shows an absorption edge around 350 nm. A direct bandgap of 2.82 and 2.96 eV was estimated for BWO-Co_3O_4 VAN and BWO thin films, respectively, by the Tauc method as shown in Fig. 5(b). The reported bandgap of Co_3O_4 is 0.75 eV based on prior literature [45]. To further understand the optical response, angular-dependent transmittance spectra of both BWO-Co_3O_4 VAN and BWO thin films were collected at different incident light angles as shown in Figs. 5(c) and 5(d), respectively. The angle-dependent transmission of both BWO-Co_3O_4 VAN and BWO thin films shows an onset point shift (marked by arrows) to lower wavelength with the increase of incident light angles, signifying highly anisotropic nature of the BWO-Co_3O_4 VAN and BWO thin films.

The optical dielectric permittivity of the BWO-Co_3O_4 VAN and BWO thin films was evaluated using a spectroscopic ellipsometer (JA Woollam RC2). The ellipsometer parameters ψ and Δ were fitted using an anisotropic model containing a mix of Lorentz and Tauc-Lorentz models to enforce the Kramers-Kronig consistency. The measurements were performed at three different angles of 55°, 65°, and 75° to improve the accuracy of the model as shown in Figs. 6(a) and 6(b). The thickness of the film was determined using the STEM images and provided as an input into the model. The simulated transmission spectra matched closely with the experimental transmission spectra, measured separately using UV–Vis spectrophotometer (Perkin Elmer Lambda 1050). Figures 6(c) and 6(d) show the calculated permittivity of the BWO-Co_3O_4 VAN and BWO thin films. Clearly, both samples show an anisotropic dielectric response with the in-plane permittivity of BWO-Co_3O_4 VAN thin film being ~ 2–3 times higher than the out-of-plane permittivity in the near infra-red wavelength regime (>1,000 nm). The anisotropy in optical permittivity is large as compared to most of the oxides which are mostly

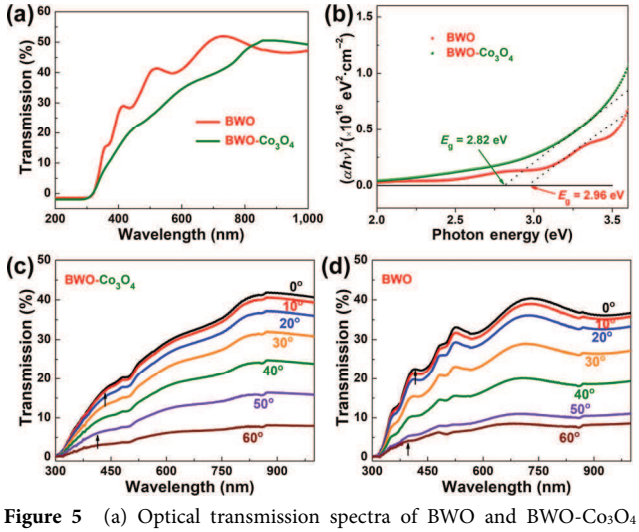

Figure 5 (a) Optical transmission spectra of BWO and BWO-Co_3O_4 VAN thin films as a function of wavelength and (b) the corresponding Tauc plots showing the bandgap of BWO and BWO-Co_3O_4 VAN thin films. Angular dependent optical transmission spectra of (c) BWO-Co_3O_4 VAN and (d) BWO thin films.

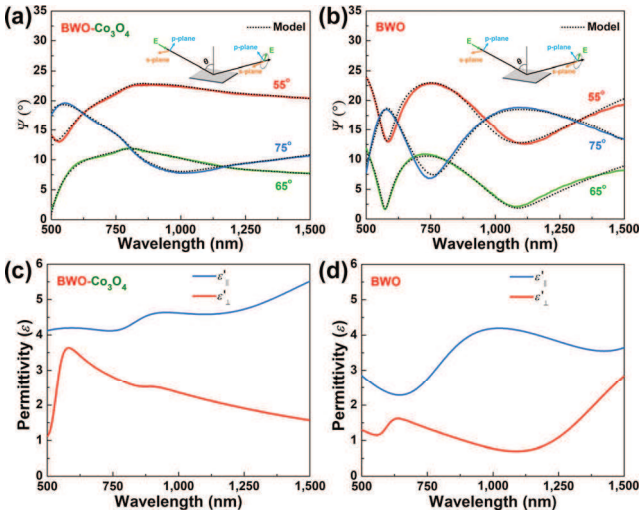

Figure 6 Experimental (solid) and fitted (dot) components of the ellipsometric parameter ψ for (a) BWO-Co_3O_4 VAN and (b) BWO thin films. The ellipsometer parameters ψ and Δ (not shown here) are measured at 55°, 65°, and 75° to improve the accuracy of the fitted model. Corresponding real part of the in-plane and out-of-plane permittivity for (c) BWO-Co_3O_4 VAN and (d) BWO thin films.

isotropic. The unique layered structure of the BWO gives rise to part of the anisotropic permittivity in the in-plane and out-of-plane directions as observed in Figs. 6(c) and 6(d). In addition, the presence of Co_3O_4 pillars with a lower E_g (0.75 eV) further gives rise to the lower out-of-plane permittivity and thus enhances the anisotropy, especially in the higher wavelength region. Interestingly, the out-of-plane permittivity continuously decreases with an increase in wavelength, leading to an increased anisotropy in the near infrared wavelength region. The nanocomposite thin film tends to behave more metallic in the out-of-plane direction as compared to the in-plane direction. Therefore, the inherent anisotropy in the BWO-Co_3O_4 VAN nanocomposite is confirmed by the anisotropic permittivity response. The fabrication of the new BWO-Co_3O_4 VAN thin film in this work with the formation of vertically aligned nanopillars plays an important role in the design of new room-temperature multiferroic materials. Magnetic elements can be introduced into the Aurivillius matrix of a ferroelectric/piezoelectric phase to fabricate nanocomposite multiferroic materials. Furthermore, the physical properties, such as magnetic and optical bandgap can be tuned by controlling the magnetic elements (Fe, Mn, Ni, etc.) and contents.

4 Conclusions

In summary, a new VAN, consisting of Co_3O_4 nanopillars and layered oxide BWO matrix, has been self-assembled by the one-step PLD growth. The new BWO-Co_3O_4 VAN structure can be well grown on different substrates and buffer layers including LAO (001), STO (001) and LSMO-buffered STO (001) substrates. Physical property measurements indicate that the new BWO-Co_3O_4 VAN structure demonstrates multifunctionalities, including room-temperature ferromagnetic and piezoelectric response as well as anisotropic optical permittivity response. This study provides a new route in designing new anisotropic and nonlinear materials by combining VAN architecture and layered oxide materials.

Acknowledgement

This work is supported by the U.S. Office of Naval Research (ONR, N00014-20-1-2600). The high-resolution TEM/STEM characterization at Purdue University is supported by the U.S. National Science Foundation (Nos. DMR-1565822 and DMR-2016453). Sandia National Laboratories is a multi-program laboratory managed and operated by National Technology and Engineering Solutions of Sandia, L. L. C., a wholly owned subsidiary of Honeywell International, Inc., for the U.S. Department of Energy's National Nuclear Security Administration under contract DE-NA0003525. This paper describes objective technical results and analysis. Any subjective views or opinions that might be expressed in the paper do not necessarily represent the views of the U.S. Department of Energy or the United States Government.

References

[1] Ramesh, R.; Spaldin, N. A. Multiferroics: Progress and prospects in thin films. *Nat. Mater.* **2007**, *6*, 21–29.

[2] Eerenstein, W.; Mathur, N. D.; Scott, J. F. Multiferroic and magnetoelectric materials. *Nature* **2006**, *442*, 759–765.

[3] Wang, J.; Neaton, J. B.; Zheng, H.; Nagarajan, V.; Ogale, S. B.; Liu, B.; Viehland, D.; Vaithyanathan, V.; Schlom, D. G.; Waghmare, U. V. et al. Epitaxial $BiFeO_3$ multiferroic thin film heterostructures. *Science* **2003**, *299*, 1719–1722.

[4] Van Aken, B. B.; Palstra, T. T. M.; Filippetti, A.; Spaldin, N. A. The origin of ferroelectricity in magnetoelectric $YMnO_3$. *Nat. Mater.* **2004**, *3*, 164–170.

[5] Marti, X.; Fina, I.; Skumryev, V.; Ferrater, C.; Varela, M.; Fábrega, L.; Sánchez, F.; Fontcuberta, J. Strain tuned magnetoelectric coupling in orthorhombic $YMnO_3$ thin films. *Appl. Phys. Lett.* **2009**, *95*, 142903.

[6] Chatterji, T.; Ouladdiaf, B.; Henry, P. F.; Bhattacharya, D. Magnetoelastic effects in multiferroic $YMnO_3$. *J. Phys. Condens. Matter* **2012**, *24*, 336003.

[7] Zhang, Q. H.; Tan, G. T.; Gu, L.; Yao, Y.; Jin, C. Q.; Wang, Y. G.; Duan, X. F.; Yu, R. C. Direct observation of multiferroic vortex domains in $YMnO_3$. *Sci. Rep.* **2013**, *3*, 2741.

[8] Zhang, W. R.; Fan, M.; Li, L. G.; Chen, A. P.; Su, Q.; Jia, Q. X.; MacManus-Driscoll, J. L.; Wang, H. Y. Heterointerface design and strain tuning in epitaxial $BiFeO_3$: $CoFe_2O_4$ nanocomposite films. *Appl. Phys. Lett.* **2015**, *107*, 212901.

[9] Pradhan, A. K.; Zhang, K.; Hunter, D.; Dadson, J. B.; Loiutts, G. B.; Bhattacharya, P.; Katiyar, R.; Zhang, J.; Sellmyer, D. J.; Roy, U. N. et al. Magnetic and electrical properties of single-phase multiferroic $BiFeO_3$. *J. Appl. Phys.* **2005**, *97*, 093903.

[10] Zhao, T.; Scholl, A.; Zavaliche, F.; Lee, K.; Barry, M.; Doran, A.; Cruz, M. P.; Chu, Y. H.; Ederer, C.; Spaldin, N. A. et al. Electrical control of antiferromagnetic domains in multiferroic $BiFeO_3$ films at room temperature. *Nat. Mater.* **2006**, *5*, 823–829.

[11] Zheng, H.; Wang, J.; Lofland, S. E.; Ma, Z.; Mohaddes-Ardabili, L.; Zhao, T.; Salamanca-Riba, L.; Shinde, S. R.; Ogale, S. B.; Bai, F. et al. Multiferroic $BaTiO_3$-$CoFe_2O_4$ nanostructures. *Science* **2004**, *303*, 661–663.

[12] Tsai, C. Y.; Chen, H. R.; Chang, F. C.; Tsai, W. C.; Cheng, H. M.; Chu, Y. H.; Lai, C. H.; Hsieh, W. F. Stress-mediated magnetic anisotropy and magnetoelastic coupling in epitaxial multiferroic $PbTiO_3$-$CoFe_2O_4$ nanostructures. *Appl. Phys. Lett.* **2013**, *102*, 132905.

[13] Murakami, M.; Chang, K. S.; Aronova, M. A.; Lin, C. L.; Yu, M. H.; Simpers, J. H.; Wuttig, M.; Takeuchi, I.; Gao, C.; Hu, B. et al. Tunable multiferroic properties in nanocomposite $PbTiO_3$-$CoFe_2O_4$ epitaxial thin films. *Appl. Phys. Lett.* **2005**, *87*, 112901.

[14] Imai, A.; Cheng, X.; Xin, H. L.; Eliseev, E. A.; Morozovska, A. N.; Kalinin, S. V.; Takahashi, R.; Lippmaa, M.; Matsumoto, Y.; Nagarajan, V. Epitaxial $Bi_5Ti_3FeO_{15}$–$CoFe_2O_4$ pillar–matrix multiferroic nanostructures. *ACS Nano* **2013**, *7*, 11079–11086.

[15] Singh, M. P.; Prellier, W.; Simon, C.; Raveau, B. Magnetocapacitance effect in perovskite-superlattice based multiferroics. *Appl. Phys. Lett.* **2005**, *87*, 022505.

[16] Neaton, J. B.; Ederer, C.; Waghmare, U. V.; Spaldin, N. A.; Rabe, K. M. First-principles study of spontaneous polarization in multiferroic $BiFeO_3$. *Phys. Rev. B* **2005**, *71*, 014113.

[17] Moriya, T. Anisotropic superexchange interaction and weak ferromagnetism. *Phys. Rev.* **1960**, *120*, 91–98.
[18] Chen, A. P.; Zhou, H. H.; Bi, Z. X.; Zhu, Y. Y.; Luo, Z. P.; Bayraktaroglu, A.; Phillips, J.; Choi, E. M.; MacManus-Driscoll, J. L.; Pennycook, S. J. et al. A new class of room-temperature multiferroic thin films with bismuth-based supercell structure. *Adv. Mater.* **2013**, *25*, 1028–1032.
[19] Li, L. G.; Zhang, W. R.; Khatkhatay, F.; Jian, J.; Fan, M.; Su, Q.; Zhu, Y. Y.; Chen, A. P.; Lu, P.; Zhang, X. H. et al. Strain and interface effects in a novel bismuth-based self-assembled supercell structure. *ACS Appl. Mater. Interfaces* **2015**, *7*, 11631–11636.
[20] Zhang, W. R.; Li, M. T.; Chen, A. P.; Li, L. G.; Zhu, Y. Y.; Xia, Z. H.; Lu, P.; Boullay, P.; Wu, L. J.; Zhu, Y. M. et al. Two-dimensional layered oxide structures tailored by self-assembled layer stacking via interfacial strain. *ACS Appl. Mater. Interfaces* **2016**, *8*, 16845–16851.
[21] Chen, A. P.; Zhou, H. H.; Zhu, Y. Y.; Li, L. G.; Zhang, W. R.; Narayan, J.; Wang, H. Y.; Jia, Q. X. Stabilizing new bismuth compounds in thin film form. *J. Mater. Res.* **2016**, *31*, 3530–3537.
[22] Nishida, M.; Sakaguchi, Y.; Takeda, H.; Nishida, T.; Uchiyama, K.; Shiosaki, T. Piezoelectric properties of bismuth layered-structure ferroelectric Bi_2WO_6 mono-domain crystals. In *Sixteenth IEEE International Symposium on the Applications of Ferroelectrics*, Nara, Japan, 2007, pp 592–593.
[23] Zeng, T.; Yan, H. X.; Ning, H. P.; Zeng, J. T.; Reece, M. J. Piezoelectric and ferroelectric properties of bismuth tungstate ceramics fabricated by spark plasma sintering. *J. Am. Chem. Soc.* **2009**, *92*, 3108–3110.
[24] Djani, H.; Hermet, P.; Ghosez, P. First-principles characterization of the $P2_1ab$ ferroelectric phase of aurivillius Bi_2WO_6. *J. Phys. Chem. C* **2014**, *118*, 13514–13524.
[25] Choi, W. S.; Chisholm, M. F.; Singh, D. J.; Choi, T.; Jellison, G. E. Jr.; Lee, H. N. Wide bandgap tunability in complex transition metal oxides by site-specific substitution. *Nat. Commun.* **2012**, *3*, 689.
[26] Choi, W. S.; Lee, H. N. Band gap tuning in ferroelectric $Bi_4Ti_3O_{12}$ by alloying with LaTMO_3 (TM = Ti, V, Cr, Mn, Co, Ni, and Al). *Appl. Phys. Lett.* **2012**, *100*, 132903.
[27] Fan, M.; Zhang, W. R.; Khatkhatay, F.; Li, L. G.; Wang, H. Y. Enhanced tunable magnetoresistance properties over a wide temperature range in epitaxial $(La_{0.7}Sr_{0.3}MnO_3)_{1-x}$: $(CeO_2)_x$ nanocomposites. *J. Appl. Phys.* **2015**, *118*, 065302.
[28] Zhang, W. R.; Li, L. G.; Lu, P.; Fan, M.; Su, Q.; Khatkhatay, F.; Chen, A. P.; Jia, Q. X.; Zhang, X. H.; MacManus-Driscoll, J. L. et al. Perpendicular exchange-biased magnetotransport at the vertical heterointerfaces in $La_{0.7}Sr_{0.3}MnO_3$: NiO nanocomposites. *ACS Appl. Mater. Interfaces* **2015**, *7*, 21646–21651.
[29] Huang, J. J.; Chen, L.; Jian, J.; Tyler, K.; Li, L. G.; Wang, H.; Wang, H. Y. Magnetic $(CoFe_2O_4)_{0.1}$-$(CeO_2)_{0.9}$ nanocomposite as effective pinning centers in $FeSe_{0.1}Te_{0.9}$ thin films. *J. Phys. Condens. Matter* **2016**, *28*, 025702.
[30] Zhang, W. R.; Jian, J.; Chen, A. P.; Jiao, L.; Khatkhatay, F.; Li, L. G.; Chu, F.; Jia, Q. X.; MacManus-Driscoll, J. L.; Wang, H. Y. Strain relaxation and enhanced perpendicular magnetic anisotropy in $BiFeO_3$: $CoFe_2O_4$ vertically aligned nanocomposite thin films. *Appl. Phys. Lett.* **2014**, *104*, 062402.
[31] Gao, X. Y.; Li, L. G.; Zhang, D.; Wang, X. J.; Jian, J.; He, Z. H.; Wang, H. Y. Novel layered $Bi_3MoM_TO_9$ (M_T = Mn, Fe, Co and Ni) thin films with tunable multifunctionalities. *Nanoscale* **2020**, *12*, 5914–5921.
[32] Wang, H.; Li, L. G.; Huang, J. J.; Gao, X. Y.; Sun, X.; Wang, H. Y. Multiferroic vertically aligned nanocomposite with $CoFe_2O_4$ nanocones embedded in layered Bi_2WO_6 matrix. *Mater. Res. Lett.* **2019**, *7*, 418–425.
[33] Chen, A. P.; Harrell, Z.; Lu, P.; Enriquez, E.; Li, L. G.; Zhang, B.; Dowden, P.; Chen, C. L.; Wang, H. Y.; MacManus-Driscoll, J. L. et al. Strain enhanced functionality in a bottom-up approach enabled 3D super-nanocomposites. *Adv. Funct. Mater.* **2019**, *29*, 1900442.
[34] Li, L. G.; Sun, L. Y.; Gomez-Diaz, J. S.; Hogan, N. L.; Lu, P.; Khatkhatay, F.; Zhang, W. R.; Jian, J.; Huang, J. J.; Su, Q. et al. Self-assembled epitaxial Au–oxide vertically aligned nanocomposites for nanoscale metamaterials. *Nano Lett.* **2016**, *16*, 3936–3943.
[35] Wang, X. J.; Wang, H. H.; Jian, J.; Rutherford, B. X.; Gao, X. Y.; Xu, X. S.; Zhang, X. H.; Wang, H. Y. Metal-free oxide-nitride heterostructure as a tunable hyperbolic metamaterial platform. *Nano Lett.* **2020**, *20*, 6614–6622.
[36] Paldi, R. L.; Wang, X. J.; Sun, X.; He, Z. H.; Qi, Z. M.; Zhang, X. H.; Wang, H. Y. Vertically aligned Ag_xAu_{1-x} alloyed nanopillars embedded in ZnO as nanoengineered low-loss hybrid plasmonic metamaterials. *Nano Lett.* **2020**, *20*, 3778–3785.
[37] von Harrach, H.; Dona, P.; Freitag, B.; Soltau, H.; Niculae, A.; Rohde, M. An integrated silicon drift detector system for FEI schottky field emission transmission electron microscopes. *Microsc. Microanal.* **2009**, *15*, 208–209.
[38] Lu, P.; Zhou, L.; Kramer, M. J.; Smith, D. J. Atomic-scale chemical imaging and quantification of metallic alloy structures by energy-dispersive X-ray spectroscopy. *Sci. Rep.* **2014**, *4*, 3945.
[39] Fan, M.; Zhang, B.; Wang, H.; Jian, J.; Sun, X.; Huang, J. J.; Li, L. G.; Zhang, X. H.; Wang, H. Y. Self-organized epitaxial vertically aligned nanocomposites with long-range ordering enabled by substrate nanotemplating. *Adv. Mater.* **2017**, *29*, 1606861.
[40] Su, Q.; Zhang, W. R.; Lu, P.; Fang, S. M.; Khatkhatay, F.; Jian, J.; Li, L. G.; Chen, F. L.; Zhang, X. H.; MacManus-Driscoll, J. L. et al. Self-assembled magnetic metallic nanopillars in ceramic matrix with anisotropic magnetic and electrical transport properties. *ACS Appl. Mater. Interfaces* **2016**, *8*, 20283–20291.
[41] Huang, J. J.; Li, L. G.; Lu, P.; Qi, Z. M.; Sun, X.; Zhang, X. H.; Wang, H. Y. Self-assembled Co-$BaZrO_3$ nanocomposite thin films with ultra-fine vertically aligned Co nanopillars. *Nanoscale* **2017**, *9*, 7970–7976.
[42] Li, L. G.; Boullay, P.; Lu, P.; Wang, X. J.; Jian, J.; Huang, J. J.; Gao, X. Y.; Misra, S.; Zhang, W. R.; Perez, O. et al. Novel layered supercell structure from Bi_2AlMnO_6 for multifunctionalities. *Nano Lett.* **2017**, *17*, 6575–6582.
[43] Seshadri, R.; Hill, N. A. Visualizing the role of Bi 6s "lone pairs" in the off-center distortion in ferromagnetic $BiMnO_3$. *Chem. Mater.* **2001**, *13*, 2892–2899.
[44] Misra, S.; Li, L. G.; Gao, X. Y.; Jian, J.; Qi, Z. M.; Zemlyanov, D.; Wang, H. Y. Tunable physical properties in $BiAl_{1-x}Mn_xO_3$ thin films with novel layered supercell structures. *Nanoscale Adv.* **2020**, *2*, 315–322.
[45] Kormondy, K. J.; Posadas, A. B.; Slepko, A.; Dhamdhere, A.; Smith, D. J.; Mitchell, K. N.; Willett-Gies, T. I.; Zollner, S.; Marshall, L. G.; Zhou, J. S. et al. Epitaxy of polar semiconductor Co_3O_4 (110): Growth, structure, and characterization. *J. Appl. Phys.* **2014**, *115*, 243708.